ANATOMICAL STRUCTURE OVERRIDES TEMPERATURE CONTROLS ON MAGNESIUM UPTAKE - CALCIFICATION IN THE ARCTIC/SUBARCTIC CORALLINE ALGAE *LEPTOPHYTUM LAEVE* AND *KVALEYA EPILAEVE* (RHODOPHYTA; CORALLINALES)

Merinda C. Nash

Walter Adey

Department of Botany, National Museum of Natural History, Smithsonian Institution, Washington, DC, USA, 20560

Author for correspondence: nashm@si.edu

Running title: Magnesium and anatomy in coralline algae

Key words: Coralline algae, calcification, biomineralization, magnesium, temperature, proxy

Abstract

Calcified coralline red algae are ecologically key organisms in photic benthic environments. In recent decades they have become important climate proxies, especially in the Arctic and Subarctic. It has been widely accepted that Magnesium content in coralline tissues is directly a function of ambient temperature, and this is a primary basis for their value as a climate archive. In this paper we show for two genera of Arctic/Subarctic corallines, *Leptophytum laeve* and *Kvaleya epilaeve,* that previously unrecognized complex tissue and cell wall anatomy bears a variety of basal signatures for Mg content, with the accepted temperature relationship being secondary. The interfilament carbonate has lower Mg than adjacent cell walls and the hypothallial cell walls have the highest Mg content. The internal structure of the hypothallial cell walls can differ substantially from the perithallial radial cell wall structure. Using high-magnification Scanning Electron Microscopy and etching we expose the nm-scale structures within the cell walls and interfilament. Fibrils concentrate at the internal and external edges of the cell walls. Fibrils ~10 nm thick appear to thread through the radial Mg-calcite grains and form concentric bands within the cell wall. This banding may control Mg distribution within the cell. Similar fibril banding is present in the hypothallial cell walls but not the interfilament. Climate archiving with corallines can achieve greater precision with recognition of these parameters.

Introduction

Understanding tissue complexity and the structural organization of cell wall calcification in coralline algae is important for many reasons, including the growing use of these organisms as climate proxies and concern for the ecological effects of ocean acidification. There is a burgeoning interest in using coralline crusts as environmental proxies for late Holocene temperature (Hetzinger et al. 2009, Gamboa et al. 2010, Halfar et al. 2010), arctic ice sheet coverage (Halfer et al. 2013) and pH changes with time (Krayesky-Self et al. 2016). Typically magnesium content is used as a key indicator of late Holocene temperature fluctuations (Adey et al. 2013). Yet despite this utilization of coralline carbonate crusts for proxy climate research, there has been little study of tissue and cellular-scale physiology as it relates to the distribution of magnesium within the crust. Nor are the basic mechanisms of calcification fully understood (Adey 1998). This is in stark contrast to the status of other calcifiers used for proxy work, e.g. corals (Barnes and Lough 1993), foraminifera (Bentov and Erez 2005) and bivalves (Wanamaker et al. 2008). However, these well-known climate proxies have little application in the Arctic Region of greatest climate change affects (Adey et al. 2013), and without a greater understanding of coralline calcification physiology, precision proxy analysis of temperature and other environmental conditions, using coralline algae, is limited.

One of the key roles of corallines is the building of carbonate substrate that underpins many ecosystems globally. For example, the thick bioherms found in coral reef structures (Adey 1978a, b, 1998), the extensive rhodolith beds off South American (Amado-Filho et al. 2012, Bahia et al. 2010) and Australian (Harvey et al. 2016) shores, maerl substrate in the Mediterranean (Martin et al. 2014) and the dominant rocky benthos

biostromes and rhodoliths in many Arctic and Subarctic environments (Adey et al. 2013). There are concerns that as atmospheric pCO_2 increases and consequent ocean acidification increases, there will be negative impacts on the capacity of corallines to continue building these important substrates (e.g. McCoy and Kamenos 2014), although there are experimental studies that find no negative impacts (e.g. Cox et al., 2017). The pace of research on the effects of temperature and climate change on coralline algae has outpaced both the published data on anatomy and our understanding of the biochemical processes controlling their carbonate skeletal building. For developing reliable past climate proxy information using corallines and anticipating future climate change impacts on these keystone calcifiers, as with any other organism, it is first necessary to understand how these algae organize their tissues, build their skeleton and control cellular-scale magnesium content.

While numerous studies of coralline growth rates under a wide range of temperature and light conditions have been published (Adey and McKibben 1970, Adey 1970, 1973, Adey and Vassar 1975, Kamenos et al. 2008, Diaz-Pulido et al. 2014, Vásquez-Elizondo & Enríquez 2016), little attempt has been made to relate this information to calcification processes. Also, it is only recently, with the use of higher magnification scanning electron microscopy (SEM) (Adey et al. 2005, 2015a) that the earlier implications of anatomical complexity (Adey 1964, 1965,1966a, Cabioch and Giraud 1986) have been fully appreciated. It has been proposed that calcification is a result of locally elevated pH during photosynthesis leading to super-saturation and associated mineral precipitation (Ries 2010). However, some parasitic corallines lack photosynthetic pigments, and have

haustoria to derive nutrition from their hosts, yet present typical tissue and calcified wall structures (Adey and Sperapani 1971, Adey et al.1974). Also, anatomical and magnesium content studies of Arctic corallines demonstrate that growth continues in Arctic winter darkness (Halfar et al. 2011, Adey et al. 2013) indicating that calcification is not likely a straight forward association with micro-saturation state, as seen in some algae (e.g., *Halimeda*, Adey 1998, Sinutok et al. 2012).

Following on from the classical coralline studies, maturing around the turn of the 19th century, Adey (1964, 1965,1966a,b) laid out the basic tissue-structured anatomy of crustose corallines, adding the epithallium, intercalary meristem and cellular elongation (while calcified) to the classical model of perithallium and hypothallium. Later, SEM (Adey et al. 2005, Adey et al.2012) demonstrated greater sub-tissue complexity and added the calcified cell wall components inner wall (IW) and interfilament (IF). It should be noted that while the interfilament is a minor component of total calcification in the species of this paper, it can be a major component in some genera (Adey et al. 2013, 2015a).

In this paper, we show for the first time the cellular-scale and anatomical controls on magnesium distribution within the carbonate skeletons of two Arctic/Subarctic coralline species. These are *Leptophytum leave* (Stromfelt) Adey, and the epiphytic (and non-photosynthetic parasitic) *Kvaleya epilaeve* Adey and Sperapani, from the northern Labrador Coast. *L. leave* is photosynthetic and forms expansive, but thin crusts (up to one mm in thickness) generally on shell fragments and pebbles in deeper water (Adey

106 1966a, 1970). *K. epilaeve* is an epiphytic parasite, lacking in photosynthetic pigment, and
107 producing hypothallial haustoria that penetrate upper perithallial cells of *L. leave* (Adey
108 and Sperapani 1971). It is similar in physiology to the North Pacific Subarctic parasite
109 *Ezo epiyessoense* (Adey et al.1974), which, along with its host *Lithophyllum yessoense*,
110 lies in a distantly related coralline group. *K. epilaeve* is the only known Arctic genus of
111 algae (Adey et al. 2008) and is absent or of very limited occurrence in Subarctic waters,
112 where the host continues to be abundant (Adey and Sperapani 1971). Understanding and
113 contrasting calcification within these two species, both growing in the same temperature,
114 light and pH conditions, offers an opportunity to examine the wide variance of Mg
115 content as a function of skeletal anatomy and metabolic processes.
116
117 **Methods**
118 *Sample collection and site information*
119 The sample was collected on 22nd July 2013, at the commencement of Arctic summer,
120 from 16-18 m depth at inner Port Manvers Bay, Labrador. The collection site lies at 56º
121 57.1' N; 61º 32.8' W., near the northern end of the 50 km long Port Manvers Run, a
122 north/south passageway inside of S. Aulatsivik Island (Fig. 1A, C). Sea ice is extensive
123 from November through early July, and the inter-island passages and bays are covered
124 with sea ice through much of that period. At the collection site, the bottom was a
125 shell/pebble gravel bed primarily of shell fragments and pebbles encrusted with *L. leave*,
126 *L. foecundum* and *Clathromorphum compactum*; scattered coarse rhodolith
127 *Lithothamnion glaciale* and *Lithothamnion tophiforme* were also present (Fig. 1B, D). *K.*
128 *epilaeve* occurred on *L. leave* and *L. leave* grew on both sides of the shell fragments.

129 Salinity was 30 and measured using electronic induction instrumentation. November to
130 July near surface water temperatures, below the sea ice, are within the -1.5 to -1.8º C
131 range. Bottom summer temperature measured at the site on 22nd July 2013 was 0.5ºC.
132 Since this is relatively early in the summer season, peak temperatures are likely to be
133 between 3-5ºC (Adey et al. 2015) with a mean growing season temperature of ~ 2 º C.
134 This mean estimate is based on measurements from eight sites in the region (182 km S to
135 35 km N) with surface to bottom temperature records for 1964 (Adey 1966c) and 2013
136 (Adey et al. 2015). These ranged from 1.9 to 5.6º C during summer at 15-20 m. The
137 snow-covered land fast sea ice overlying the gravel rhodolith bed from which the samples
138 were taken likely precludes significant solar energy from reaching the bottom for eight
139 months of each year.
140
141 The original sample is 2013-11(1) at the National Museum of Natural History.
142
143 **Analytical methods**
144 *Scanning electron microscopy- energy dispersive spectroscopy (SEM-EDS)*
145 The CCA sample was fractured, mounted using carbon tape and platinum coated prior to
146 scanning electron microscopy energy dispersive spectroscopy (SEM-EDS). For these
147 analyses, we used a Zeiss UltraPlus field emission scanning electron microscope
148 (FESEM) equipped with an HKL electron backscatter diffraction (EBSD) operated at 15
149 kV, 11 mm working distance. SEM was carried out at the Australian National University
150 Centre for Advanced Microscopy. SEM-EDS was used for spot analyses to quantify the
151 elemental composition of representative parts of the CCA crust. A range of SEM settings

were used for imaging. The more common secondary (SE) electron showing topography, backscatter electron imaging (BSE) which shows higher magnesium areas as darker carbonate and is useful for rapid visual identification of mineral distribution.

A second round of EDS was undertaken using a NOVA NanoSEM FEI at the National Museum of Natural History's Department of Mineralogy. Typically EDS measurements are made using 15 kV (Nash et al. 2011) so that there is sufficient energy to dislodge electrons from a range of elements, e.g. from lighter magnesium up to heavier strontium. The EDS beam interacts with a roughly spherical-shaped region of carbonate beneath the surface. This region is referred to as the interaction volume. At 15 kV the interaction volume is ~ 3 μm in diameter whereas the average cell wall thickness ranges from only 500 nm up to ~2 μm (occasionally thicker, up to 3 μm). Interfilament in these species may be only a few grains wide, 200-500 nm up to 2 μm. These narrow areas of interest in contrast to the larger beam interaction volume, pose a problem for obtaining accurate Mg measurements for only cell wall or interfilament. For example, a measurement of the cell wall may include minor amounts of carbonate from the adjacent interfilament and vice versa. Generally even with this beam crossover, in our experience 15 kV is sufficient to identify a significant offset in magnesium while still collecting information that may be of interest such as strontium levels. However, where there are only a few grains of interfilament, as in the *L. leave,* the 3 μm interaction volume is problematic. A range of EDS settings were tested aiming to reduce the beam interaction volume so that Mg content for each the cell wall and the interfilament could be individually measured without the beam crossing into the adjacent substrate. A setting of 7 kV, working distance

6.4 mm and 1 nA current was used to measure the interfilament grains in the *L. leave* with a count time of 20 seconds. The sample was carbon coated. This was calculated to have an interaction volume of <1 μm. These results are reported separately to the main data set.

Sample preparation

Initially the crust was fractured using shears and mounted in superglue. After first imaging of the fractured crust, the sample was polished using 2000 gsm wet and dry sandpaper then sonic cleaned in unbuffered deionized water for 2 minutes. This preparation was used for SEM EDS measurements; 8-9 measurements were made for each carbonate type of interest. Subsequently the sample was sonic cleaned in unbuffered deionized water for 20 minutes. The deionized water has a pH of ~6.5. When cleaned for 2 minutes the surface is very lightly etched allowing differentiation between different Mg-calcite morphologies without altering the measured Mg content. After cleaning for 20 minutes there is a visible difference in the surface with much of the interfilament Mg-calcite and smaller grains removed allowing imaging of nm scale cellular structures.

X-ray diffraction methods

Powder XRD was carried out using a SIEMENS D501 Bragg-Brentano diffractometer equipped with a graphite monochromator and scintillation detector, using CuKα radiation. A subsample was broken off the edge of the crust. This piece included *L. leave* with surficial *K. epilaeve*. The sample was ground using a mortar and pestle. Fluorite was added as an internal standard. The sample was not bleached and acetone was not added

198 during the grinding as this has been found to occasionally induce alteration and
199 precipitation of other minerals in other coralline samples we have worked with. Scan
200 interpretation for mol% $MgCO_3$ followed the methods described by Nash et al. (2013).
201
202 *Terminology*
203 In this paper, we rename the inner wall the cell wall and retain the terminology
204 interfilament, noting this is equivalent to the middle lamella in higher plants (Esau 1953);
205 interfilament has also been referred to as interstitial (Ragazzola et al. 2016). We use the
206 abbreviations PCW and PIF (perithallial cell wall and perithallial interfilament) and
207 HCW and HIF (hypothallial cell wall and interfilament) to designate the carbonate wall
208 components.
209
210 **Results**
211 *SEM imaging overview*
212 The specimen of *L. laeve* encased an aragonite carbonate shell. (Fig. 2A). The crust is
213 approximately 500 μm thick (Fig. 2B) with a basal hypothallus ~80 μms thick. *K.*
214 *epilaeve* has been considered to be an adelphoparasite, a species very closely related to its
215 host. Although diminutive, and superficially appearing as scattered white sand grains, *K.*
216 *epilaeve* can densely coat *L. leave*. Although often appearing as densely crowded
217 conceptacles, it can possess the full basic array of anatomical features: hypothallium,
218 perithallium and epithallium (the latter mostly absent, Adey and Sperapani 1971) (Fig.
219 2B). *L. laeve* typically has an epithallium that is one cell layer of rounded ovoid, thin
220 walled cells that are often absent in SEM sections. The *K. epilaeve* grows directly on the
221 *L. laeve* meristem (Fig. 2C, D) and there was no evidence of excavation required (by

222 borers or grazers), prior to settlement. This suggests that unlike the typical sloughing
223 relationship with epiphytes wherein epithallium builds up under the epiphyte until it
224 sloughs off, the *L. leave* does not recognize *K. epilaeve* as foreign. The perithallial cell
225 walls of *L. laeve* contain radially-oriented grains of Mg-calcite; the interfilament is thin
226 and has carbonate grains randomly orientated in a plane parallel to the filament axis or
227 cell top/ bottom. The interfilament shows up strongly as stripes on vertical fracture
228 sections (Figs. 2B, C). Note for easiest viewing of the fine structures, the figure images
229 are best viewed on screen rather than in print.
230
231 The first layer formed by the *K. epilaeve* has angular grains parallel to the *L. laeve*
232 surface (Fig. 2E). The bottom part of the cell wall is without radial structure and has
233 submicron beads appearing to calcify along and within organic fibrils (Fig. 2E). Organic
234 fibrils are visible between the basal layer of *K. epilaeve* carbonate grains and the
235 meristem of the *L. leave* (Fig. 2F) suggesting a method of attachment in addition to the
236 haustoria developed by some hypothallial cells (Adey and Sperapani 1971). There were
237 no haustoria visible in our SEM sample. Fine radial grains typically observed in cells of *L.*
238 *leave* beneath the meristem were not apparent in the cell walls of the *L. laeve* meristem
239 (Fig. 2E,F) suggesting this surficial carbonate may have been altered or remineralised
240 during the attachment process.
241
242 *SEM-EDS*
243 Measurements for magnesium content in *Leptophytum leave* were undertaken on both the
244 upper (side with conceptacles) and under (without conceptacles) crusts (Fig. 3A, D). The

245 parasite, *Kvaleya epilaeve* was present on both surfaces (Fig. 2A, B Fig. 3A).
246 Measurements of *K. epilaeve* were made on the underside.
247
248 The Mg content of the perithallial and hypothallial cell walls of *L. leave* was measured
249 (Fig. 3 A-D) as well as what appeared to be a transitional cell type between the basal
250 hypothallus and the typical perithallial cells (Fig. 2 D-F). These transitional cells are
251 within the perithallus but have thin cell walls similar to the hypothallial cells. There are
252 clear visual differences between the cell walls of the three cell types. The perithallial cell
253 walls are 1-2 μms wide with clearly radial Mg-calcite (Fig. 2B, F). The basal
254 hypothallial cells are elongated relative to the perithallial cells and their cell walls are
255 narrower and do not always show radial cell wall structure (Fig. 2C). The transitional
256 cells have elongate cells relative to the perithallus but less so than the hypothallus, and
257 their cell walls are thinner, ~ 0.5 – 1 μm and do not show radial structures. The
258 interfilament of *L. laeve* has only a single layer of Mg-calcite grains (Fig. 2B, F), as noted
259 above showing as a thin line on longitudinal axial fractures; fractures along the
260 interfilament appear as conspicuous vertical stripes (Figs. 2C).
261
262 The *K. epilaeve* in the portion of the sample mounted for SEM did not present the typical
263 elongated hypothallial cells as shown by Adey and Sperapani (1971), as this cut is not
264 longitudinally placed on a growing lobe. The key difference between the perithallus of
265 the *L. laeve* and *K. epilaeve* was the presence of wide (1-2 μms) areas of interfilament in
266 the *K. epilaeve* (Fig. 3F, 4A, B). In many corallines (Adey et al. 2005), including the *L.*
267 *laeve* studied for this paper there is only a single layer of interfilament grains, and these

are present as vertical stripes on vertical fractures (Fig. 3B). EDS measurements were taken for both the *K. epilaeve* cell wall and interfilament (Fig. 4A, B). As the interaction volume of the EDS beam is ~ 3 μms (Methods) and the cell wall and interfilament thickness range from 1-3 μms, the values measured for both may include small amounts of the other, although every effort was made to place the beam on the widest part of the appropriate band. A second set of measurements was taken for the *L. leave* cell wall and interfilament using lower kV and the results are reported separately.

Mg content

Bulk whole sample content of Mg, determined by powder XRD was 10.8 mol% $MgCO_3$ (Mg/Ca 0.13). The EDS-determined average Mg content ranged from 9.1 (*K. epilaeve* Perithallial interfilament) to 16.7 mol% $MgCO_3$ (*L. leave* upper Hypothallial cell wall), (Table 1, Fig.6). The highest measured individual Mg content, 19.6 mol% $MgCO_3$, was in the *L. leave* upper crust HCW. Generally the Mg content of interfilament was lower than cell walls, and perithallial cell walls had the highest Mg content. The lowest values were for the *K. epilaeve* PIF and PCW, 9.1 and 10.1 mol% $MgCO_3$ respectively, not significantly different at significance level of 0.05 but are significantly different at significance level of 0.1 ($p= 0.068$) (Table 2). Keeping in mind the values for the cell wall and interfilament include a small amount of carbonate from the other, we consider the $p=0.068$ result likely does represent a true significant difference between the two. The PCW for the *L. laeve* was slightly higher at 11.2 and 12.9 mol% $MgCO_3$ (under and upper crust respectively), these were not significantly different from each other ($p=0.112$). The combined average of the upper and under *L. leave* cell walls (12.2 mol% $MgCO_3$)

291 was significantly higher (p=0.025) than the *K. epilaeve* cell wall. However, comparing
292 only the *L. leave* cell wall of the under crust, the same side as the *K. epilaeve,* there was
293 no significant difference (p=0.124). The greatest difference between the upper and under
294 *L. laeve* crust was found between the hypothallial cell walls. The under HCW averaged
295 12.3 mol% $MgCO_3$, whereas the upper HCW was 4.4 mol% higher at 16.7 mol% $MgCO_3$.
296 The upper HCW was significantly higher than the *L. leave* PCW's but not different from
297 the transitional CW's (15.6 mol% $MgCO_3$). Based on the graph in figure 5 this upper
298 range of Mg would equate to temperatures above 9.3°C, more than double the known
299 summertime highs at the sampling site.
300
301 The results for comparison of the cell wall and interfilament grains in the *L. leave* using 7
302 kV showed the interfilament, 8.5 mol% $MgCO_3$ (n=6), was significantly lower (p=0.001)
303 than the cell wall, 11.1 mol% $MgCO_3$ (n=8).
304
305 **Structural features**
306 *Cell wall*
307 Within the radial Mg-calcite structure (PCW) of the *K. epilaeve*, a concentric banding
308 pattern is present (Fig. 7 A-C). The radial Mg-calcite grains are not always one
309 continuous long grain. The banding is aligned to the presence of organic fibrils that
310 appear regularly throughout the PCW (Fig. 7B). Organic fibrils, ~10 nm thick, are
311 parallel to the cell wall edges. These are spaced 30-40 nm apart throughout the middle of
312 the cell wall. It appears that the fibrils are mineralized. At the outer edges of the cell wall
313 the number of fibrils increases and appear as a dense mesh approaching a membrane (Fig.

7B, C) that is infilled with carbonate. The parallel fibrils are connected to the radial Mg-calcite grains, appearing as if to continue through the grain (Fig. 7C), similar to fence wire threading through fence posts at pre-defined spacing. There are also fibrils that drape over the grains. Where the fibrils concentrate to a mesh, this is also calcified but with smaller grains without regular shape. In the *K. epilaeve* interfilament (PIF), the grains are aligned to the cell wall surface (Fig. 7C). Fibrils also run through the PIF and attach to the interfilament grains but not with the regular pattern seen in the cell wall. Looking at a cross section of the cell wall from the top down (Fig. 7D), the fibrils can be seen to form a dense mesh.

Similar features are visible in the *L. laeve* PCW (Fig. 8A, B), although the organic fibrils are not as well exposed. Possibly these cell wall grains are less susceptible to dissolution in the etching treatment making it more difficult to expose the organic features. The radial cell wall grains appear anchored to the external edge of the cell wall, immediately adjacent the interfilament.

After etching for 20 minutes, more of the organic fibrils are exposed in the *K. epilaeve* interfilament (Fig. 9A) revealing a porous membrane. PIF grains have angular edges in contrast to the rounded sides of the cell wall grains. The *L. laeve* perithallial interfilament has rice-grain shaped Mg-calcite flattened against the external side of the cell wall (Fig. 9B) with attachment fibrils. Fibrils are visible stretching between the flattened interfilament grains on adjacent cells (Fig. 9C).

Hypothallial cell walls at 200-500 nm wide are much thinner than perithallial cell walls (Fig. 10 A-C). The HCW internal structure appears roughly radial (Fig. 10 A- C). But, the radial structure is not always well developed with parts of the HCW exhibiting a distinct break down the middle of the radial structures (Fig. 10C). There are fibrils parallel to the cell wall appearing to go through the wall grains similarly to the perithallial cell walls. Interfilament grains are present, as in perithallial cells (Fig. 10B, C). The HCW wall can have two clearly defined morphologies (Fig. 10C). The wall adjacent to the interfilament is narrowest at ~200 nm, has closely spaced organic fibrils and is poorly calcified compared to the inner part of the wall (300-400 nm wide) and appears more like a mineralized membrane. The wider inner part of the cell wall has radial grains but without

347 the well-defined shape of the PCW radial grains. Similar to the perithallial cell walls,
348 there are fibrils appearing to thread through the hypothallial cell wall grains.
349
350 The transitional cells between the hypothallus and perithallus have features from both
351 types present (Fig. 10D). The cell walls can be narrow, <200 nm, poorly mineralized
352 similarly to the outer part of the hypothallial cell wall. Parts of the cell wall resemble the
353 perithallial cell walls, with radial grains and wall width of nearly 1 μm, although along
354 the same wall this changes to ~200 nm wide and a poorly mineralized membrane. The
355 parallel fibrils are also present within the transitional cell walls. Interfilament grains are
356 present comparably to those between hypothallial and perithallial cells.
357
358 **Discussion**
359 *Site temperature, ecology and growth*
360 The site of collection for this specimen (Fig. 1A) is a pavement of coralline encrusted,
361 roughly flat to ovoid shells and pebbles often with dish shapes. Many, such as the
362 specimen employed in this study have a concave surface (due to the original mollusk
363 shape). The benthic surface that we show in figure 1B is likely quite stable with time in
364 the moderate reversing tidal current environment of the site. The conceptacles of *L. leave*,
365 requiring considerable solar energy for construction; all appear on the upper side of the
366 specimen and further assist our determination of orientation. Since the sea ice does not
367 clear the area until late June or early July, solar energy has already peaked, by the time
368 the benthos at 15-17 m receives significant light. Effectively, the growing season is July
369 through November, and with a mean growing season temperature of < 2º C. Based on the

370 lateral growth rates (5-7 μm/day) found by Adey (1970), a season of lateral growth would
371 provide less than one mm of extension. As we discuss below, the vertical growth in this
372 species is slower than the lateral growth. The layering seen in figure 2B likely represents
373 4-5 years of vertical growth. At 80-100 μm of perithallial addition/year, this relates well
374 to the 100-200 μm /year found with extensive data in the same region for
375 *Clathromorphum compactum* (Adey et al. 2015b).
376
377 Considering that *Leptophytum leave* crusts can be many cm broad and rarely exceed 500
378 μm in thickness, except by overgrowing of earlier crusts, it can be assumed that after
379 initial formation, upwards perithallial growth is either very slow, perhaps limited by the
380 development of conceptacles for which considerable photosynthate must be dedicated. *L.*
381 *leave* is a deep water species (Adey 1966a, b, 1968, 1971) and requires little solar energy
382 to grow and carry out its life cycle; however, as shown by Adey (1970), the rate of
383 hypothallial extension falls with light reduction, and it would be expected that growth on
384 the underside of a shell-encased fragment would be present but less than that on the upper
385 surface.
386
387 *Temperature and magnesium*
388 One of the challenges using samples collected at a single point in time is that the growth
389 history cannot always be precisely tied to previous points in time and temperature. As
390 discussed in the previous section, this crust likely represents 4-5 years of growth. Thus
391 the XRD mol% $MgCO_3$ is an average for that period. The individual EDS measurement

392 spots cannot be tied to a particular time of year or temperature. However, the annual
393 temperature range is not large, estimated to be ~ 4 ºC across the growing season.
394
395 The XRD Mg content is within the range for average winter and summer Mg contents for
396 *Clathromorphum compactum* collected from Arctic Bay, Kingitok and Quirpon (Halfar et
397 al. 2011, 2013). The EDS-determined average Mg content for each carbonate type had a
398 range of 7.6 mol% $MgCO_3$, from 9.1 (*K. epilaeve* interfilament) to 16.7 mol% $MgCO_3$ (*L.*
399 *laeve* upper crust hypothallus). The *L. laeve* upper hypothallus has 84% more Mg than
400 the *K. epilaeve* interfilament. Although the exact time and temperature of formation for
401 each component is not known, the temperature range (~4 ºC) alone is highly unlikely to
402 explain the Mg difference. Studies on Mg content in CCA for temperature proxies have
403 used regressions with temperature records to determine a range of responses from 0.266
404 mol % (Williamson et al. 2014), ~1.0 (Halfar et al. 2000; Darrenougue et al. 2013) to
405 1.76 mol% $MgCO_3$ (Kamenos et al. 2008) per degree celsius of temperature increase.
406 Only the Kamenos et al. (2008) calibration is close to explaining the range here.
407 However, that calibration was for branches of the rhodolith *Lithothamnion glaciale*.
408 Using temperature calibrations for crust CCA in experimental treatments, where
409 temperature was the only condition changed (Diaz-Pulido et al. 2014; Nash et al. 2016), a
410 calibration of 0.33 mol%/°C is obtained. This rate is in agreement with results from
411 Williamson et al. (2014), Chave and Wheeler (1964) and Adey (1965). Using 0.33, a shift
412 of 7.6 mol% equates to 23°C of change, nearly four times greater than the maximum
413 annual range at this site. The magnesium offsets in different parts of the crust are clearly
414 aligned to anatomical features and not controlled by temperature. This proposal is

415 supported by recent results for species of CCA *Phymatolithon* that also demonstrated
416 anomalously higher Mg in hypothallial cells across four species collected from differeing
417 locations (Nash and Adey 2017). Within these offsets there may still be a response to
418 temperature over the seasons, but it was beyond the capacity of this study to investigate
419 seasonal changes. It is noteworthy that the upper crust hypothallus average of 16.7 mol%
420 $MgCO_3$ is equivalent to new surface crust of tropical *Porolithon onkodes* grown at 30° C
421 (Diaz Pulido et al. 2014).
422
423 *Structural features*
424 There are three main types of calcified structures within the vegetative tissues of
425 *Leptophytum leave* and *Kvaleya epilaeve*: (1) the radial Mg-calcite within the cell walls
426 of the perithallium, (2) the interfilament in both the perithallium and hypothallium and
427 (3) the thin hypothallial cell walls. Each has distinctively different features and
428 magnesium content. The more elongate (and thinner-walled) cells of the hypothallus have
429 been reported for other species of Melobesioideae (Adey 1964, 1965, 1966a). However,
430 this is the first study to show that the internal cell wall Mg-calcite structure and their
431 magnesium content differs from perithallial cell wall. Probably these thinner elongated
432 hypothallial cell walls are a result of relatively rapid growth during lateral extension.
433 There are numerous examples documenting higher Mg in parts of crusts that have grown
434 faster during the warmer seasons (e.g. *Clathromorphum compactum* and *C. nereostratum*
435 by Adey et al. 2013). In this case the Mg increase is associated with anatomical change,
436 not temperature. The mechanistic process by which more Mg is incorporated into the
437 HCW and how this relates to growth rate is not known. The *K. epilaeve* perithallial cells

had lower Mg than the *L. leave* perithallial cells. Cabioch and Giraud (1986) described the *perithallial* cells as being a later stage of development than *epithallial* cells. Epithallial cells do not have fully developed rounded cell walls of the perithallial cells (Adey 2015a, b). Although Mg-content of epithallial carbonate is lower than the perithallial values (Diaz-Pulido et al. 2014, Nash et al. 2015, 2016), the lower Mg measured here is not considered a result of different cell type as the *K. epilaeve* cell walls have the radial calcite similarly to the perithallial *L. Leave*, indicating that these are similarly well developed. Considering the time of collection in early summer, it is quite possible that the *K. epilaeve* growth closest to the *L. leave* surface was laid down closer to winter and in cooler temperatures, this being a likely explanation for the lower Mg content.

Calcification and photosynthesis

The parasitic epiphyte *K. epilaeve* is not known to photosynthesize. The similarity of cell wall and interfilament features to those of the photosynthesizing host, *L. leave*, suggests that the precipitation of the Mg-calcite is not directly driven by photosynthesis as has been suggested for coralline algae (Ries 2010) and demonstrated for calcifying green algae *Halimeda*, (e.g. Adey 1998, Sinutok et al. 2012). Rather, considering also the evidence for continued calcification during the Arctic winter (Halfar et al. 2011, Adey et al. 2013), it seems likely the first control is the provision of the organic substrate that subsequently either becomes calcified or induces calcification. This does not negate the possibility of increased calcification as photosynthetic rates increase (e.g. Borowitzka 1981).

461 *Banding and magnesium uptake*

462 The concentric banding of organic fibrils within the perithallial cell wall may offer
463 insight into controls on Mg variation within the cell wall. The dominant visual
464 morphological pattern is the radial Mg-calcite crystals. In contrast, other work indicates
465 the dominant pattern of Mg distribution within the cell may be unrelated to the radial
466 features. Concentric zonations of higher Mg content have been shown, using back scatter
467 electron imaging, in cell walls of tropical *Porolithon onkodes* (Nash et al. 2011).
468 Ragazzola et al. (2016) using NanoSIMs, also showed clear concentric banding of Mg
469 within summer cell walls of *Lithothamnion glaciale*. These published observations
470 together with the results in this study suggest there could be a strong organic control on
471 Mg distribution within the cell, with this being related to the concentric fibrils. Possibly
472 the fibril organics enable higher Mg incorporation than the organics involved in the radial
473 structures. Ragazzola et al. (2016) further documented a decreased prominence of Mg
474 banding in winter cells of *L. glaciale* and for those grown in CO_2 enriched conditions.
475 Results from our study offer an insight as to possible temperature or CO_2-driven
476 ultrastructure changes that may result in decreased Mg content. If the banded fibrils
477 observed in this study are normally similarly present in the *L. glaciale,* then an absence of
478 the Mg bands for their winter and elevated CO_2 treatment suggests that these fibrils could
479 either be absent, or the organic structure or composition has changed and no longer
480 enables elevated Mg.

481

482 *Relevance to Climate Archiving*

483 This study has several implications for climate archiving using corallines. Most
484 importantly, anatomical controls can override temperature influences on Mg composition.
485 We do not suggest current studies are inadequate because the finer scale (submicron)
486 scale variations are not captured. These fine scale variations will not change the general
487 trends or conclusions. Rather, we suggest caution regarding interpretation of data where a
488 change in Mg is visibly associated with a change in cell type as temperature may not be
489 the only possible driver of Mg change. While hypothallial areas can usually be easily
490 excluded from most climate archiving (but see Bougeois et al. 2015), less obvious
491 anatomically different tissues such as the elevated Mg transitional cell walls may not be
492 noticeable at low magnification. This may lead to a false positive result identifying such a
493 region as reflecting a time of higher temperature. As well as these tissue-scale differences,
494 the cellular scale differences may also need to be considered. Any seasonal change in
495 relative proportion of CW to IF can shift the [Mg] in absence of any temperature-
496 influenced change. For example if CW = 10 mol% $MgCO_3$ and IF = 8 mol% $MgCO_3$,
497 and crust changes from 90:10 CW:IF to 50:50 this would equate to a change in of 9.8 to 9
498 mol% for measurements of bulk crust (i.e. spot sizes larger than the cell size, or smaller
499 spot sizes averaged without reference to their anatomical placement). This change
500 equates to a 2-3 degrees using a temperature calibration of 0.33 mol% $MgCO_3$ °C. Should
501 the difference in cell wall and interfilament mol% $MgCO_3$ be larger, then the total
502 average will change more substantially. Furthermore, the bulk magnesium results for
503 different CCA species with differing proportions of cell wall:interfilament from the same
504 temperature environments will have a range of non-temperature related Mg content that is
505 controlled by the cell wall:interfilament. This change in structure, if seasonally correlated,

506 will be indirectly related to temperature, but there may be other influences such as light.
507 For example, CCA continue to grow in darkness using stored photosynthates, after ice
508 sheets have formed above (Halfar et al. 2013), however, it is not known if a switch to
509 using stored energy results in any anatomical changes. If there were changes, these would
510 only be indirectly related to temperature. More recently Sletten et al. (2017) found
511 anatomical changes (banding) in *Lithothamnion* rhodoliths were unrelated to temperature
512 and proposed these were driven by differences in light exposure. Thus, the best CCA
513 temperature climate archives, as compared to seasonal archives, are likely to be those
514 with the least seasonally varying ultrastructure changes.
515
516 Understanding the combined contribution of anatomical and temperature changes to
517 measured magnesium may help explain the variation of Mg-temperature calibrations in
518 the published literature. Typically it is the rhodoliths that show the highest response of
519 Mg to temperature, e.g. *Lithothamnion glaciale* at 1- 1.76 mol% $MgCO_3$ (Halfar et al.
520 2000; Kamenos et al. 2008) per degree celsius of temperature increase compared to
521 *Clathromorphum compactum* at 0.7 mol% $MgCO_3$ (Halfar et al. 2010). The *L. glaciale*
522 has distinct seasonal changes shifting to a clear band of elongated cells during summer.
523 The rhodolith summer cells have similarities in appearance to the hypothallial cells in this
524 study. Possibly the higher measured Mg in the long cells of the rhodolith is a result in
525 part of a switch towards a more perithallial style cell and may not be entirely temperature
526 related. This proposition is supported by Sletten et al. (2017) who found a switch to
527 elongated cells with higher Mg that was unrelated to seasonality. In contrast, anatomical
528 changes in *C. compactum* (Adey et al. 2013) are not so extreme.

529

530 *Suggestions for improving analytical methods*

531 Our work is ongoing in this area of research and as more species and ultrastructures are
532 studied we expect to be able to provide more detailed guidance on utilizing Mg from
533 CCA for climate proxies. However, in the interim, there are several steps that could be
534 incorporated into routine analyses to improve the accuracy of Mg climate proxies. Firstly,
535 it should become a routine part of analyses that the ultrastructure is assessed to determine
536 if the ratio of cell wall to interfilament carbonate changes regularly with seasons. Second,
537 when possible as well as the larger spot sizes used in sampling transects, e.g. 10-20 μms,
538 make discrete spot analyses using the smallest reliable interaction volume possible to
539 determine indicative Mg offsets between the cell wall and interfilament so that this can be
540 adjusted for if necessary, in the final interpretation. Third, ensure that hypothallial growth
541 is not included in sampling transects. Usually the basal hypothallus is easily avoided, but
542 secondary hypothallus and transitional cells may be harder to avoid without careful SEM
543 analysis.

544

545 **Conclusion**

546 It appears that within these CCA, there is a strong control on the uptake of Mg in relation
547 to the different anatomical components. This is in contrast to the suggestion by Ries
548 (2010), based on Mg:Ca in seawater manipulation experiments, that corallines exert little
549 or no control over their Mg uptake other than to specify the polymorph. Recent work
550 indicates that the interfilament and perithallial carbonate react similarly to temperature,
551 but the responsive hypothallial carbonate is inconclusive (Nash and Adey 2017). It would

552 be interesting to identify if each of interfilament, perithallial and hypothallial cell walls
553 reacted similarly to changes in seawater Mg:Ca, or if there were differences in anatomical
554 controls. Crucially, it is necessary to keep in mind the biological controls on Mg uptake
555 when using CCA Mg changes as a climate proxy.
556
557 While the focus of this study has been the distribution of Mg with different anatomical
558 features, the high-magnification images are the first to show the cellular-scale organic
559 structures together with the carbonate components. The orientation of the crystals in the
560 interiflament and the cell walls are in agreement with lower-magnification SEM studies
561 on a range of algal species (Cabioch and Giraud 1986, Adey et al. 2013). The
562 combination of gentle etching and high-magnification SEM has revealed previously
563 unknown features such as the fibrils threading through the radial Mg-calcite (Fig. 7C).
564 Further, showing that the Mg content varies with anatomical features suggests that the
565 calcification may be a different process, or have different controls, for each carbonate
566 type. This adds an extra level of complexity when considering how environmental
567 changes, such as increasing temperature, may impact on the capacity of the CCA to
568 continue their important substrate provision ecological role.
569
570 **Acknowledgments**
571 Thanks to the Centre for Advanced Microscopy at the Australian National University and
572 the Mineral Sciences department at the Smithsonian Institution for assistance with SEM-
573 EDS.
574

575 **References**

576 Adey, W. 1964. The Genus *Phymatolithon* in the Gulf of Maine. *Hydrobiologia*
577 24:377-420.

578 Adey, W. 1965. The Genus *Clathromorphum* in the Gulf of Maine. *Hydrobiologia*
579 26:539-573.

580 Adey, W. 1966a. The Genera *Lithothamnium, Leptophytum* (nov. gen.) and
581 P*hymatolithon* in the Gulf of Maine. *Hydrobiologia* 28:321-368.

582 Adey, W. 1966b. The Genus *Pseudolithophyllum* in the Gulf of Maine.
583 *Hydrobiologia* 27:479-597.

584 Adey, W. 1966c. The Distribution of Saxicolous Crustose Corallines in the
585 Northwestern North Atlantic. *J. Phycol.* 2:49-54.

586 Adey, W. 1970. The Effects of Light and Temperature on Growth Rates in
587 Boreal-Subarctic Crustose Corallines. *J. Phycol.* 6:269-276.

588 Adey, W. 1973. Temperature Control of Reproduction and Productivity in a
589 Subarctic Coralline Alga. *Phycologia* 12:111-118.

590 Adey, W. 1978a. Coral Reef Morphogenesis: A Multidimensional Model.
591 *Science* 202:831-837.

592 Adey, W. 1978b. Algal Ridges of the Caribbean Sea and West Indies. *Phycologia*
593 17:361-367.

594 Adey, W. 1998. Coral Reefs: algal structured and mediated ecosystems in shallow,
595 turbulent alkaline seas. *J. Phycol.* 34:393-406.

596 Adey, W. & D. McKibbin. 1970. Studies of the Maerl Species of the Ria de Vigo.
597 *Bot. Mar.* 8:100-106.

598 Adey, W. & C. Sperapani. 1971. The Biology of *Kvaleya epilaeve*, A New
599 Parasitic Genus and Species of Corallinaceae. *Phycologia* 10:29-42.
600 Adey, W., T. Masaki & H. Akioka. 1974. *Ezo epiyessoense*, A New Parasitic Genus and
601 species of Corallinaceae. *Phycologia* 13:329-344.
602 Adey, W. & J. M. Vassar. 1975. Colonization, Succession and Growth Rates of
603 Caribbean Crustose Corallines. *Phycologia* 14:55-69.
604 Adey, W., Y. Chamberlain, & L. Irvine. 2005. A SEM-Based Analysis of the
605 Morphology, reproduction and ecology of *Lithothamnion tophiforme* Unger
606 (Corallinales, Rhodophyta), an Arctic coralline. *J. Phycol*. 41:1010-1024.
607 Adey, W., Lindstrom, S., Hommersand M. & Muller, K. 2008. The biogeographic origin
608 of Arctic endemic seaweeds: A thermogeographic view. *J. Phycol.* 44:1384-1394.
609 Adey, W., Halfar, J. & Williams, B. 2013. The coralline genus *Clathromorphum* Foslie
610 emend Adey; biological, physiological and ecological factors controlling
611 carbonate production in an Arctic/Subarctic climate archive. *Smithsonian*
612 *Contributions to the Marine Sciences* 40:1-83.
613 Adey, W., Hernandez-Kantun, J. J., Johnson, G. & Gabrielson, P. 2015a. DNA
614 sequencing, anatomy and calcification patterns support a monophyletic, Subarctic,
615 carbonate reef-forming *Clathromorphu*m (Hapalidiaceae, Corallinales,
616 Rhodophyta). *J. Phycol.* 51:189-203.
617 Adey, W., Halfar, J., Humphreys, A. Belanger, D., Gagnon, P. & Fox, M. 2015b.
618 Subarctic rhodolith beds promote longevity of crustose coralline algal buildups
619 and their climate archiving potential. *Palaios* 30:281-293.

620 Amado-Filho, G., Moura, R., Bastos, A., Salgado, L., Sumida, P., Guth, A., Francini-
621 Filho, R., Pereira-Filho, G., Abrantes, D., Brasileiro, P., Bahia, R., Leal, R.,
622 Kaufman, L., Kleypas, J., Farina, M. & Thompson, F. 2012. Rhodolith Beds are
623 major CaCO3 bio-factories in the Tropical South West Atlantic. *Plos One* 7
624 (4):e35171.
625 Bahia, R., Abrantes, D., Brasileiro, P., Pereira-Filho, G. & Amado-Filho, G. 2010.
626 Rhodolith bed structure along a depth gradient on the northern coast of Bahia
627 State, Brazil. *Brazilian J. Oceanography* 58:323–337.
628 Barnes, D. J., & Lough, J. M. 1993. On the nature and causes of density banding in
629 massive coral skeletons. *J. Exp. Mar. Biol. Ecol.* 167:91-108.
630 Bentov, S., & Erez, J. 2005. Novel observations on biomineralization processes in
631 foraminifera and implications for Mg/Ca ratio in the shells. *Geology* 33:841-844.
632 Borowitzka, M. A. 1981. Photosynthesis and Calcificaton in the Articulated Coralline
633 Red Algae *Amphiroa anceps* and *A. foliacea*. Mar. Biol. 62:17-23.
634 Bougeois, L., Williams, B., Halfar, J., Konar, B., Adey, W., Kronz, A. & Wortmann, U.G.
635 2015. Does the coralline alga *Leptophytum fœcundum* (Kjellman) capture
636 paleoenvironmental variability in the Arctic Ocean? *Arctic, Antarctic, and Alpine*
637 *Research* 47:375-387.
638 Chave, K. & B. Wheeler. 1965. Mineralogical changes during growth in the red alga
639 *Clathromorphum compactum. Science* 147:621.
640 Cox, T. E., M. Nash, F. Gazeau, M. Déniel, E. Legrand, S. Alliouane, P. Mahacek, A. Le
641 Fur, J-P. Gattuso, & S. Martin. 2017. Effects of in situ CO2 enrichment on

642 Posidonia oceanica epiphytic community composition and mineralogy. *Mar.*
643 *Biol.* 164:103.
644 Darrenougue, N., De Deckker, P., Payri, C., Eggins, S., & Fallon, S. 2013. Growth and
645 chronology of the rhodolith-forming, coralline red alga Sporolithon
646 durum. *Marine Ecology Progress Series* 474:105-119.
647 Diaz-Pulido, G., Nash, M.C., Anthony, K.R., Bender, D., Opdyke, B.N., Reyes-Nivia, C.
648 & Troitzsch, U., 2014. Greenhouse conditions induce mineralogical changes and
649 dolomite accumulation in coralline algae on tropical reefs. *Nature*
650 *communications*, *5*.
651 Esau, K. 1953. Plant Anatomy. John Wiley and Sons. New York. 735 pp.
652 Nash, M. C., Opdyke, B. N., Troitzsch, U., Russell, B. D., Adey, W. H., Kato, A., Diaz-
653 Pulido G., et al. 2013. Dolomite-rich coralline algae in reefs resist dissolution in
654 acidified conditions. *Nat. Clim. Change* 3:268-272.
655 Halfar, J., Zack, T., Kronz, A., & Zachos, J. C. 2000. Growth and high-resolution
656 paleoenvironmental signals of rhodoliths (coralline red algae)- A new biogenic
657 archive. *J. Geophysical Research* 105:22-107.
658 Gamboa, G., Halfar, J., Hetzinger, S., Adey, W., Zack, T., B. Kunz, B., & Jacob, D. 2010.
659 Mg/Ca ratios in coralline algae as proxies for NW Atlantic temperature variations.
660 *J. Geophysical Research-Oceans* 115:1-12.
661 Halfar, J., Hetzinger, S., Adey**,** W., Zack, T., Gamboa, G., Kunz, B., Williams, B., Jacob,
662 D. 2010. Coralline algal growth increment widths archive North Atlantic climate
663 variability. *Palaeogeography, Palaoeoclimatology, Palaeoecology* 302:71-80

664 Halfar, J., Adey, W., Kronz, A., Edinger, E., & W. Fitzhugh, W. 2013. Unprecedented
665 sea-ice decline archived by novel multi-century annual-resolution algal proxy.
666 *PNAS* 110: 197837-19741.
667 Harvey, A. S., Harvey, R. M., & Merton, E. 2016. The distribution, significance and
668 vulnerability of Australian rhodolith beds: a review. *Marine and Freshwater*
669 *Research* doi.org/10.1071/MF15434.
670 Hetzinger, S., Halfar, J., Kronz, A., Steneck, R.S., Adey, W., Lebednik, P. A. & Schone,
671 B. R. 2009. High-Resolution Mg/Ca Ratios in a coralline Red Alga As a Proxy
672 for Bering Sea Temperature Variations from 1902-1967. *Palaios* 24:406-412.
673 Kamenos, N., Cusack, M., & Moore, P. G. 2008. Coralline Algae Are Global
674 Paleothermometers with Bi-Weekly Resolution. *Geochimica et Cosmochimica*
675 *Acta* 72:771–779.
676 Kamenos, N. A., & Law, A. 2010. Temperature controls on coralline algal skeletal
677 growth. *J. Phycol.* 46:331-335.
678 Krayesky-Self, S., Richards, J., Rahmatian M., & Fredericq, S. 2016. Aragonite infill in
679 overgrown conceptacles of coralline Lithothamnion spp (Hapalidaceae,
680 Hapalidiales, Rhodophyta): new insights in biomineralization and
681 phylominerology. *J. Phycol.* 52:161-173.
682 Martin, C. S., Giannoulaki, M., De Leo, F., Scardi, M., Salomidi, M., Knittweis, L., Pace,
683 M. L. et al. 2014. Coralligenous and maërl habitats: predictive modelling to
684 identify their spatial distributions across the Mediterranean Sea. *Sci. Rep.* 4.

685 McCoy, S. J., & Kamenos, N. A. 2015. Coralline algae (Rhodophyta) in a changing
686 world: integrating ecological, physiological, and geochemical responses to global
687 change. *J. Phycol.* 51:6-24.
688 Nash, M.C. & Adey, W., 2017. Multiple phases of mg□calcite in crustose coralline algae
689 suggest caution for temperature proxy and ocean acidification assessment: lessons
690 from the ultrastructure and biomineralisation in Phymatolithon (Rhodophyta,
691 Corallinales). *J. Phycol*. In press. 10.1111/jpy.12559
692 Nash, M. C., Troitzsch, U., Opdyke, B., Trafford, J., Russell, B., & Kline, D. 2011. First
693 discovery of dolomite and magnesite in living coralline algae and its
694 geobiological implications. *Biogeosciences*. 8, 3331-3340.
695 Nash, M. C., Opdyke, B. N., Wu, Z., Xu, H. & Trafford J. M. 2013. Simple X-ray
696 diffraction techniques to identify Mg calcite, dolomite, and magnesite in tropical
697 coralline algae and assess peak asymmetry. *J. Sed. Res.* 83:1085-1099.
698 Nash, M. C., Uthicke, S., Negri, A.P., & Cantin, N. E. 2015. Ocean acidification does not
699 affect magnesium composition or dolomite formation in living crustose coralline
700 algae, *Porolithon onkodes* in an experimental system. *Biogeosciences* 12:5247-
701 5260.
702 Nash M.C., Martin S., Gattuso J-P. 2016. Mineralogical response of the Mediterranean
703 crustose coralline alga *Lithophyllum cabiochae* to near-future ocean acidification
704 and warming. *Biogeosciences Discussions* doi:10.5194/bg-2016-160.
705 Ragazzola, F., Foster, L. C., Jones, C. J., Scott, T. B., Fietzke, J., Kilburn, M. R., &
706 Schmidt, D. N. 2016. Impact of high CO_2 on the geochemistry of the coralline
707 algae *Lithothamnion glaciale*. *Scientific reports*, *6*, 20572.

708 Ries, J. 2010. Review: Geological and Experimental Evidence for Secular Variation in
709 Seawater Mg/Ca (Calcite-Aragonite Seas) and Its Effects on Marine Biological
710 Calcification. *Biogeosciences,* 7:2795–2849.
711 Sletten, H. R., Andrus, C. F. T., Guzmán, H. M.,, & Halfar, J. 2017. Re-evaluation of
712 using rhodolith growth patterns for paleoenvironmental reconstruction: An
713 example from the Gulf of Panama. *Palaeogeography, Palaeoclimatology,*
714 *Palaeoecology* 465:264-277.
715 Sinutok, S., Hill, R., Doblin, M. A., Kühl, M., & Ralph, P. J. 2012. Microenvironmental
716 changes support evidence of photosynthesis and calcification inhibition in
717 *Halimeda* under ocean acidification and warming. *Coral Reefs* 31:1201-1213.
718 Sherman, C.E., Fletcher, C., Rubin, K., Simmons, K. & Adey, W. 2014. Sea-level and
719 reef accretion history of Marine Oxygen Isotope Stage 7 and late stage 5 based on
720 age and facies of submerged late Pleistocene reefs, Oahu, Hawaii. *Quaternary Res*.
721 81:138-150.
722 Sletten, H.R., Andrus, C.F.T., Guzmán, H.M. & Halfar, J., 2017. Re-evaluation of using
723 rhodolith growth patterns for paleoenvironmental reconstruction: An example
724 from the Gulf of Panama. *Palaeogeography, Palaeoclimatology,*
725 *Palaeoecology*, 465:264-277.
726 Vásquez-Elizondo, R.M. and Enríquez, S., 2016. Coralline algal physiology is more
727 adversely affected by elevated temperature than reduced pH. *Scientific reports*, *6*,
728 p.19030.
729 Wanamaker, A., Kreutz, K., Schone, B., Pettigrew, N., Borns, H., Introne, D., Belknap,
730 D., Maasch, K. & Feindel, S. 2008. Coupled North Atlantic slope water forcing

on Gulf of Maine temperatures over the past millennium. *Climate Dynamics* 31:183-194.

Williamson, C. J., Najorka, J., Perkins, R., M. L. Yallop, M. L. & Brodie, J. 2014. Skeletal mineralogy of geniculate corallines: providing context for climate change and ocean acidification research. *Marine ecology progress series* 513:71-84.

Tables

	K.epilaeve		*L. laeve*					
	IF	CW	CW Under	CW Upper	CW comb.	Under Hyp.	Upper transit.	Upper Hyp.
mol% $MgCO_3$	9.1%	10.1%	11.2%	12.9%	12.2%	12.3%	15.6%	16.7%
St. Dev.	1.0%	1.2%	1.2%	2.5%	2.2%	0.7%	1.7%	1.7%
Mg/Ca	0.100	0.113	0.126	0.149	0.138	0.140	0.185	0.200

Table 1: SEM-EDS results. Conversion of mol% to Mg/Ca is included.

	Average mol% and n	*K. epilaeve* IF	*K. epilaeve* CW	*L. laeve* under CW	*L. laeve* upper CW	*L. leave CW both*	*L. laeve* under Hyp.	*L. laeve* upper Hyp.
K. epilaeve IF	9.1 % n=9							
K. epilaeve CW	10.1% n=8	**0.069**						
L. laeve under CW	11.2% n=8		0.129					
L. laeve upper CW	12.9% n=9		**0.012**	0.112				
L. leave CW both	12.2% n=17		**0.024**					
L. laeve under Hyp.	12.3% n=8			**0.052**	0.470	0.914		
L. laeve upper Hyp.	16.7% n=8					**<0.001**	**<0.001**	
L. laeve upper trans.	15.6% n=8					**<0.001**	**<0.001**	0.259

Table 2: T-test *p* values for 15 kV spot EDS.

741 **Figures**

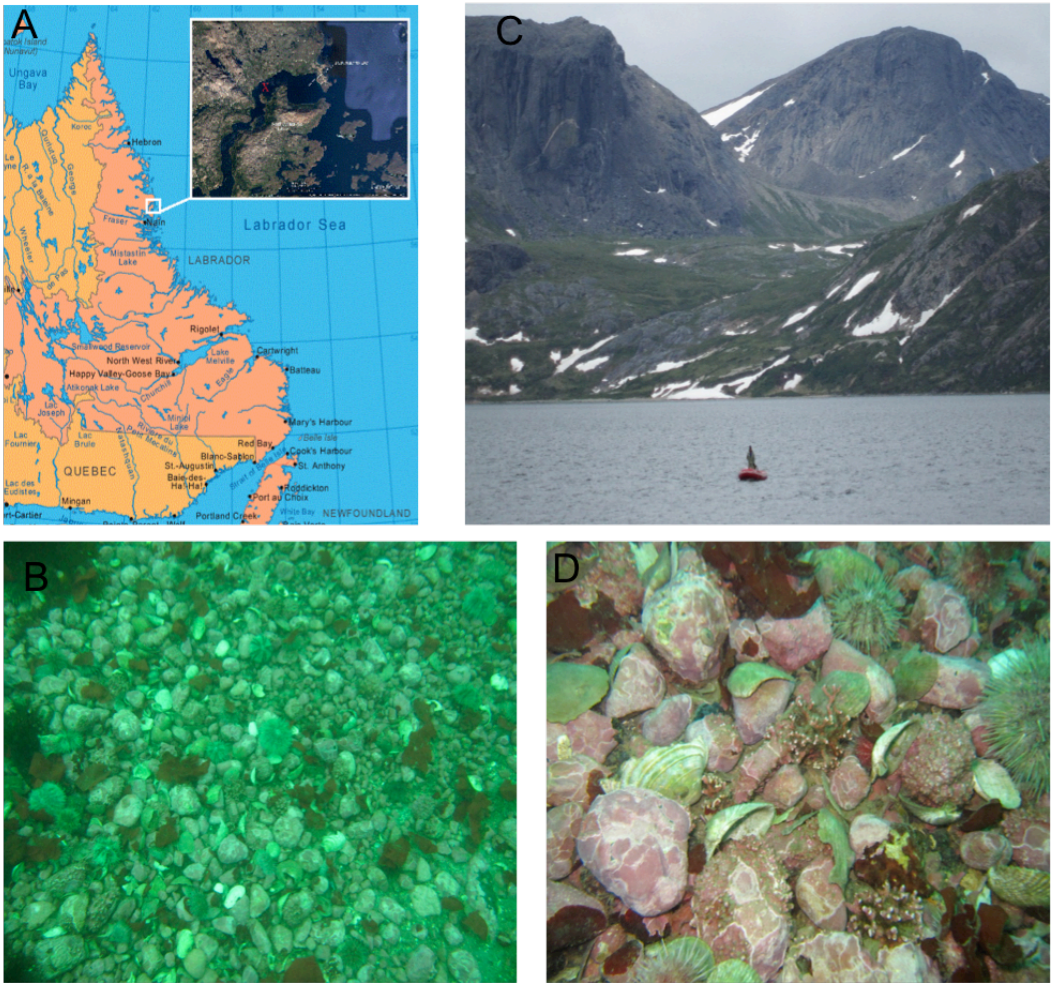

742

743 Figure 1: A. Port Manvers Bay Station, Labrador. B. Pebble/shell bottom with occasional rhodoliths at 15-

744 17 m. Coralline covered pebbles range from about 5-10 cm diameter. C. Collecting site in western Port

745 Manvers Bay. D. Close-up of bottom shown in figure 1C.

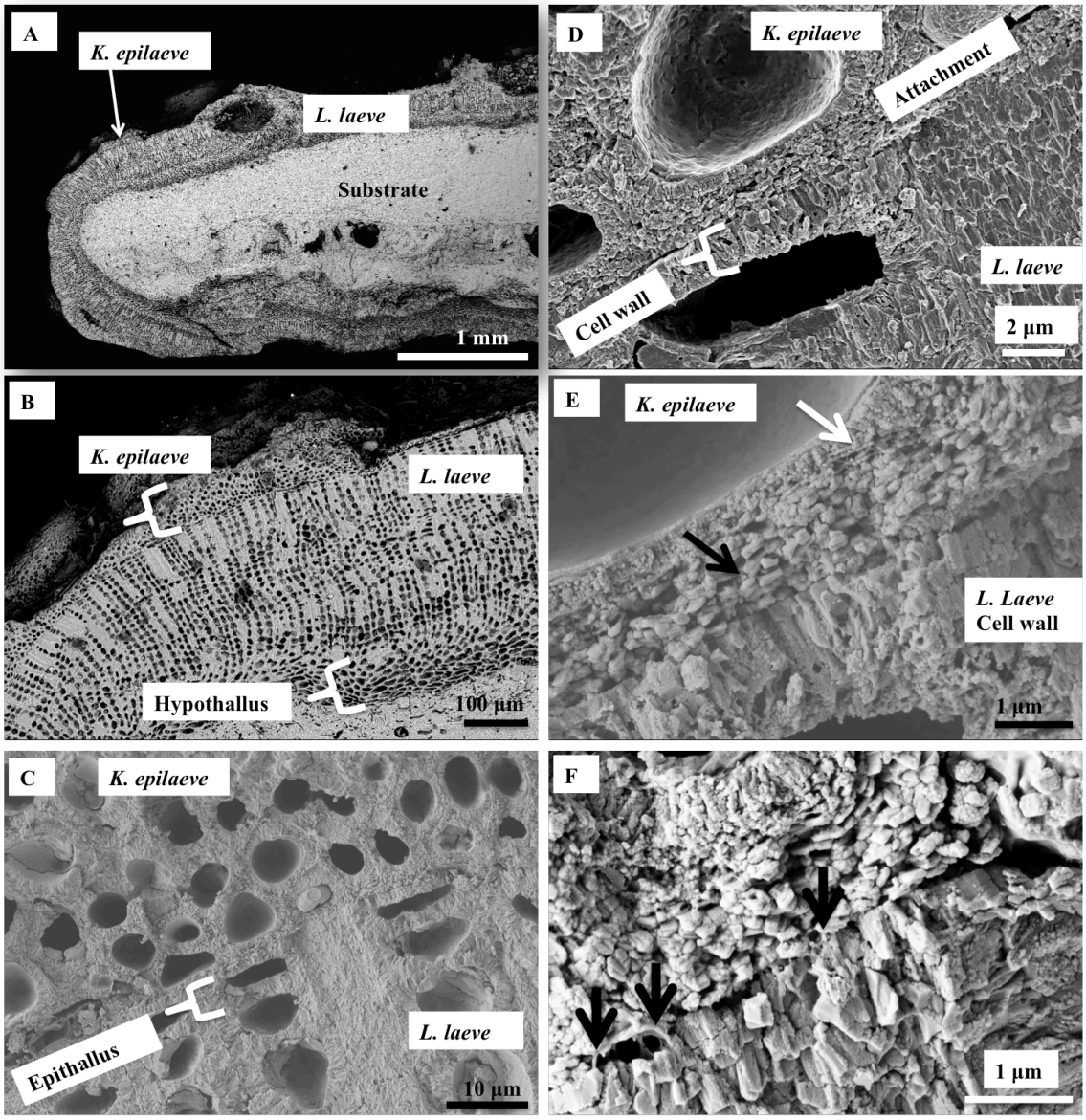

Figure 2: Overview of *K. epilaeve* on *L. laeve*. **A**. Overview (BSE). *L. laeve* has been partly overgrown by *K. epilaeve*. **B**. Closer up (BSE) *K. epilaeve* has a very thin perithallium with thicker buildup for its conceptacle. **C**. Close up (SE) and **D** showing attachment zone of *K. epilaeve* hypothallus on the epithallus of the *L. laeve*. **E**. (SE) The cell wall in the *L. laeve* is roughly radial whereas the *K. epilaeve* cell wall does not appear properly mineralized with nm-scale beads of Mg-calcite along what appears to be organic fibrils (white arrow). The *K. epilaeve* Mg-calcite layer at the attachment zone has coarse angular grains roughly parallel to the *L. laeve* surface (black arrow). **F**. (SE) Organic fibrils are visible (black arrows) between the base of the *K. epilaeve* and the surface of the *L. laeve* suggesting this is the attachment mechanism.

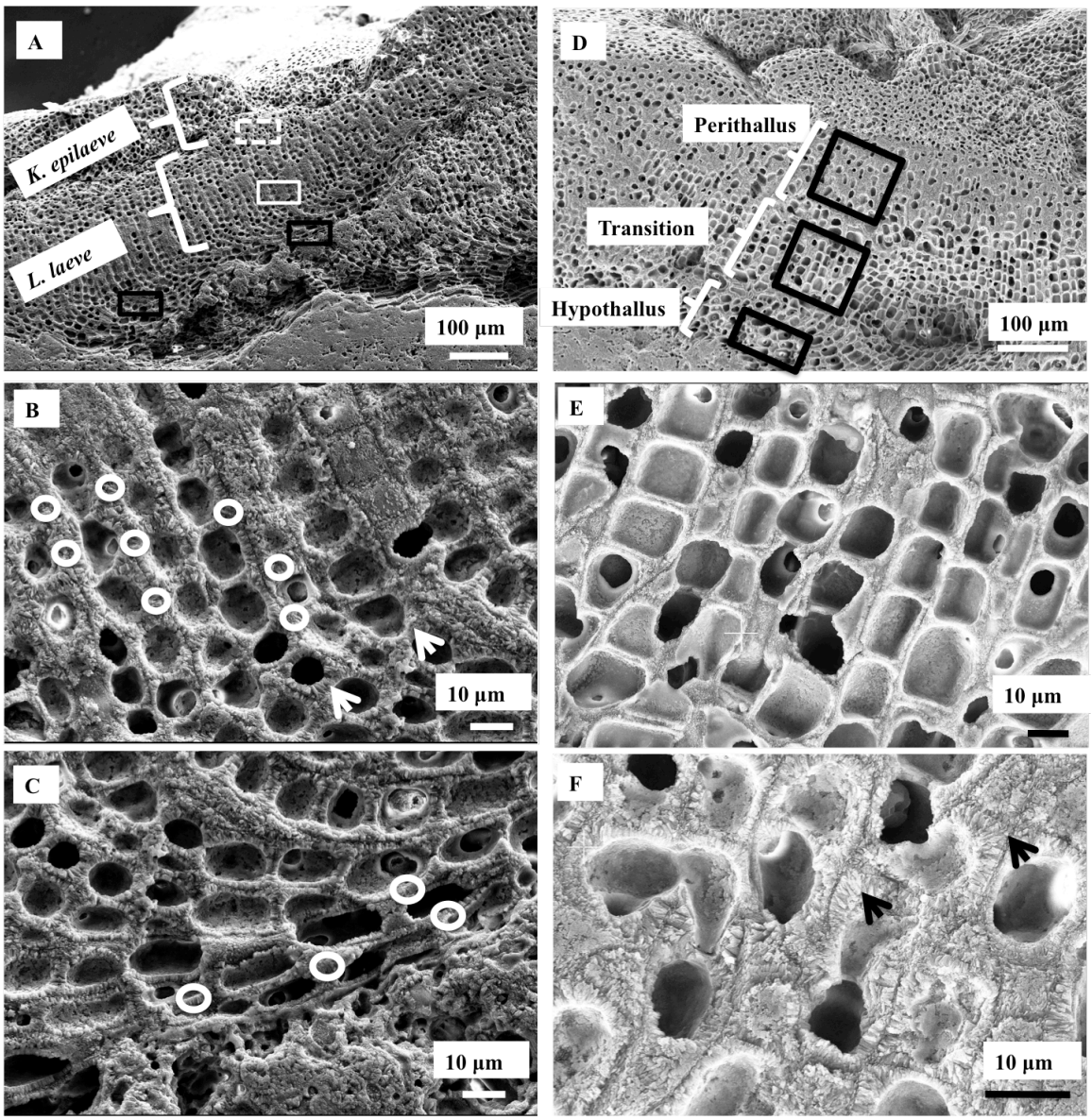

Figure 3: Overview of *L. laeve* and *K. epilaeve* and EDS sites (white circles) in *L. laeve*. **A-C**. Sites on the underside of the pebble. **D-F**. Sites on the upper side of the pebble. **A**. White dashed box- cell wall and interfilament in *K. epilaeve*. White box– perithallial cell wall *L. laeve*. Black box- hypothallus *L. laeve*. **B.** EDS sites for cell wall measurements of *L. laeve*. Circle size indicates approximate area of measurement (3 µms). Cell wall radial Mg-calcite (arrowheads). **C**. EDS sites for hypothallus (right box in A). **D**. EDS sites on sample upper side for *L. laeve*. **E.** *L. leave.* **F**. *L. leave.* Cell walls in upper side are visually comparable to cell walls in underside with radial Mg-calcite (arrowheads) in cell walls and minimal interfilament.

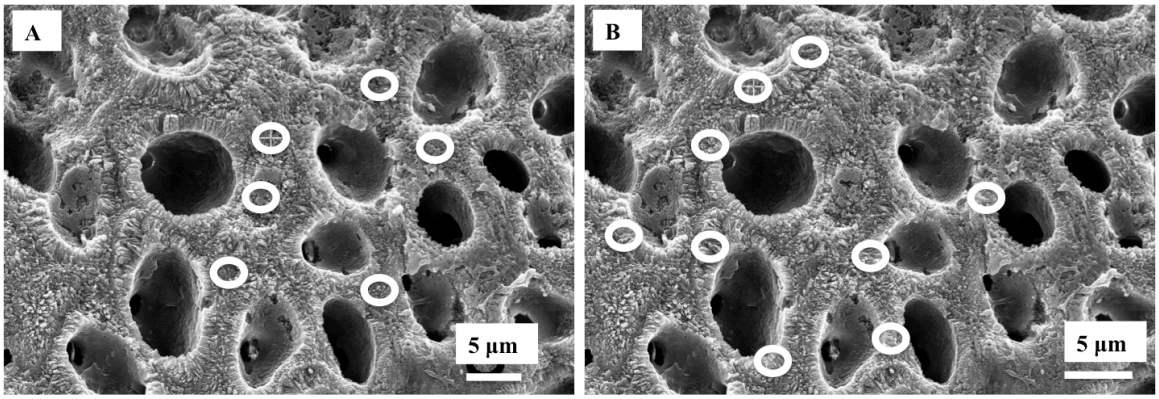

763

764 Figure 4: Detail of EDS sites in *K. epilaeve* (dashed white box in Fig. 2A) **A**. EDS sites (white circles) for

765 interfilament. **B**. EDS sites for cell wall.

766

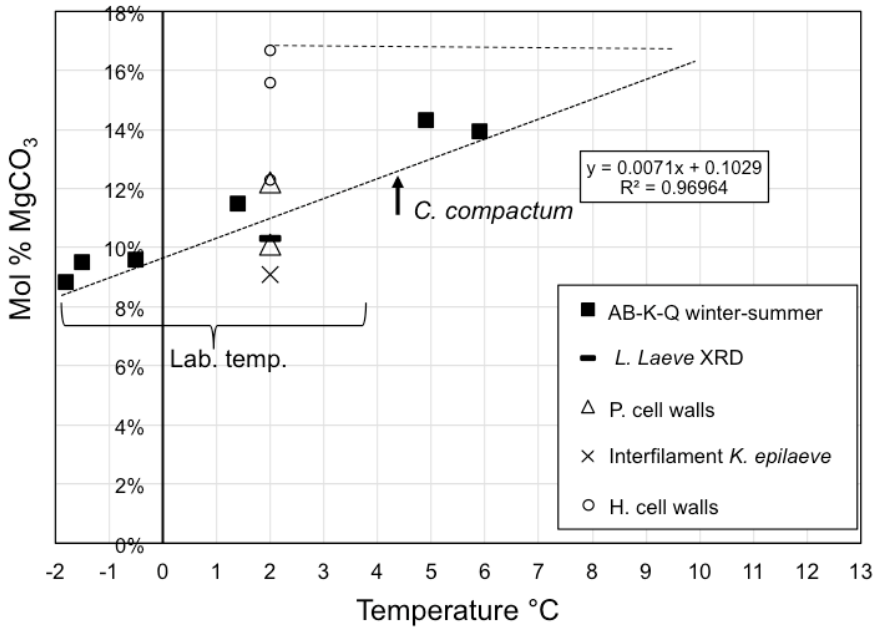

767

768 Figure 5: *L. Leave* and *K. epileave* Mg content relative to *Clathromophum compactum* from Arctic Bay,

769 Kingitok and Quirpon (Halfar et al. 2010, 2013). Lab – Labrador sea. Heavy dashed line- best fit for *C.*

770 *compactum*. Light dashed line- indicates the temperature equivalent on the *C. compactum* line for the *L.*

771 *leave* hypothallial Mg-content.

772

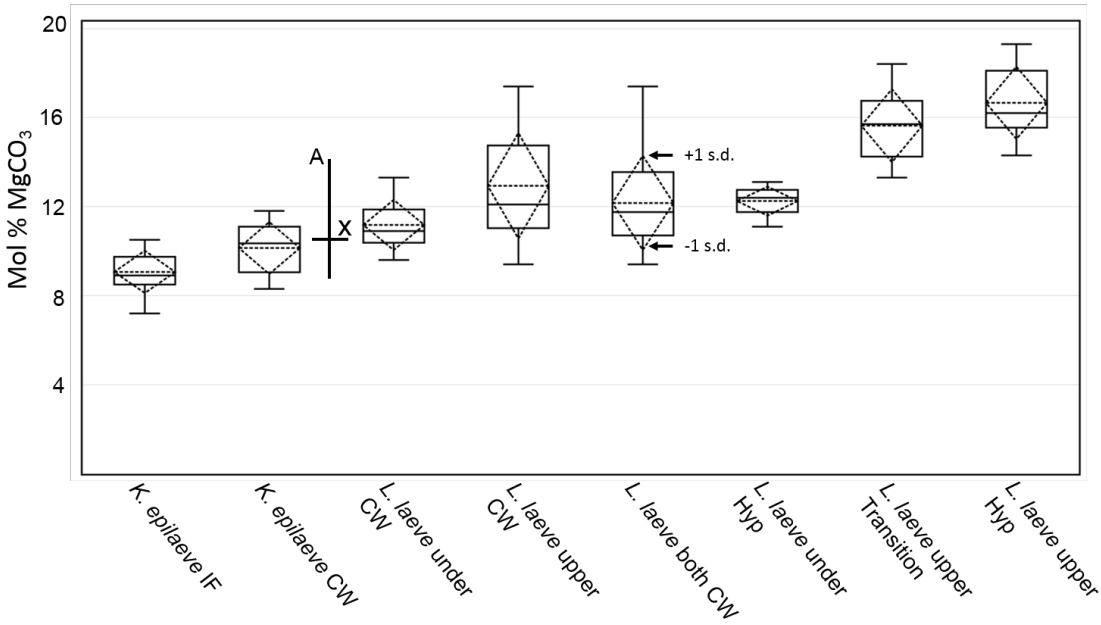

773

774 Figure 6: Box plot of EDS mol% $MgCO_3$ results. Box represents the 2nd and 3rd quartiles. The lower and

775 upper bars are the minimum and maximum values (excluding an outlier for *L. laeve* under cell wall). The

776 solid middle line within the box is the median value and the dash middle line the average. The dashed

777 diamond box represents one standard deviation. The drawn-on cross represents the XRD mol% (X) and the

778 seasonal range (A) of mol% for the Arctic Bay – Kingitok – Quirpon dataset in figure 5.

779

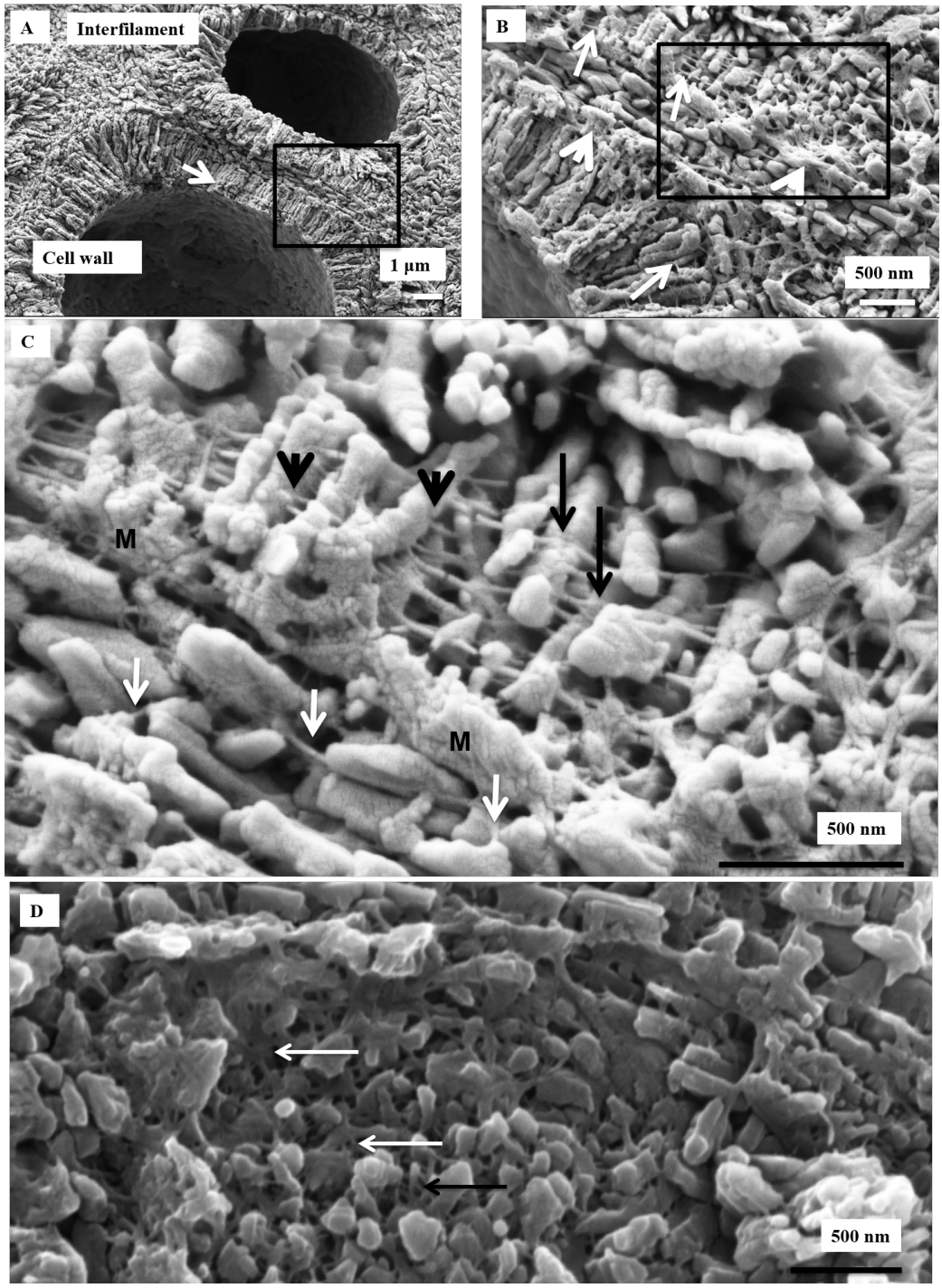

780

781 Figure 7: *K. epilaeve* cell wall structure. Crust polished and cleaned for 2 minutes. **A**. Cell walls have radial

782 Mg-calcite whereas the interfilament grains are orientated either parallel to the filament axis or randomly

783 within the corner junctions. Within the radial cell walls a secondary concentric banding pattern is visible

784 (white arrow). Black box enlarged in B. **B**. Organic fibrils, ~10nm wide, run parallel to cell wall edges

785 (black arrows). Fibrils are concentrated along the outer of the cell wall (white arrows). Black box enlarged
786 in C. **C**. The cell wall fibrils appear to string through the centre of the radial grains (black arrowheads),
787 Other fibrils drape over the grains (black arrows). Fibrils are present in the interfilament (white arrows). M
788 – mineralized membrane. **D**. Plan view of cell wall grains. Organic fibrils form a dense mesh (white
789 arrows).
790

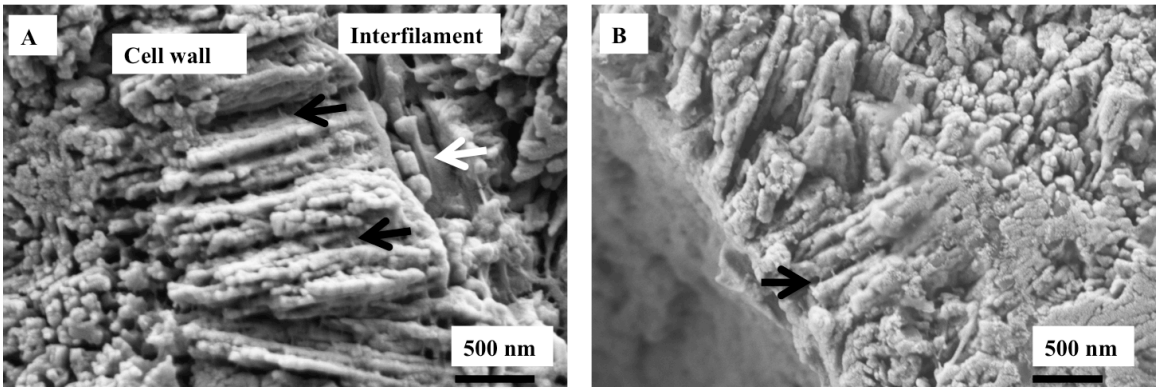

791
792 Figure 8: *L. laeve* cell wall structure. A. Cleaned for 2 minutes. Cell wall radial crystals are 1.5 μm length
793 cylindrical grains. Fibrils are present (black arrows) but not as easy to see as in the *K. epilaeve*.
794 Interfilament grains parallel to cell wall with organic fibrils (white arrows) also running parallel to cell wall.
795 B. Etched for 20 minutes. Fibrils appear similarly as in the *K. epilaeve* with the fence post-wire structure
796 (black arrows).
797

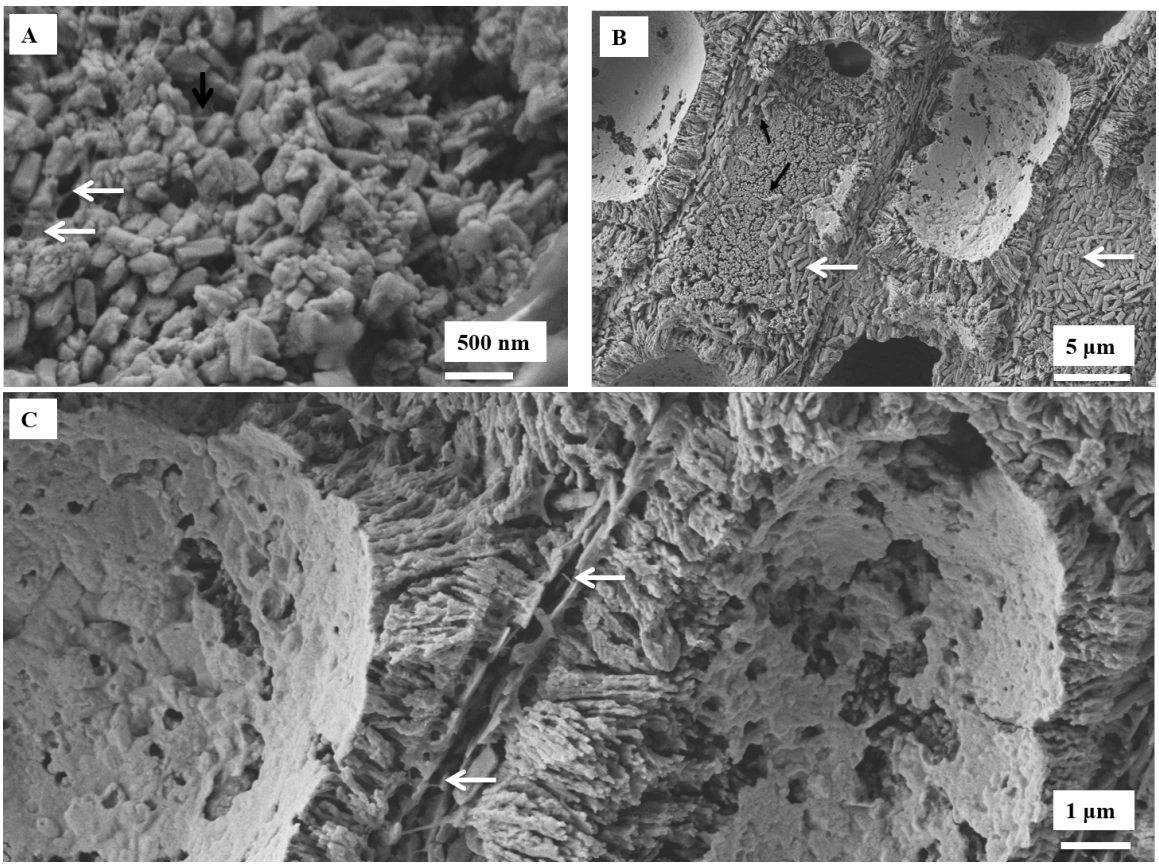

Figure 9: Interfilament structures in *K. epilaeve* (A) and *L. laeve* (B, C). **A**. *K. epilaeve* etched for 20 minutes. Fibrils (black arrow) and porous membrane (white arrows). **B**. *L. Laeve* etched for 20 minutes. Interfilament grains are flattened against the external sides of the cell wall (white arrows) attached by fibrils (black arrows). **C**. Fibrils visible stretched across the space between cell walls with 2 layers of interfilament grains (white arrows).

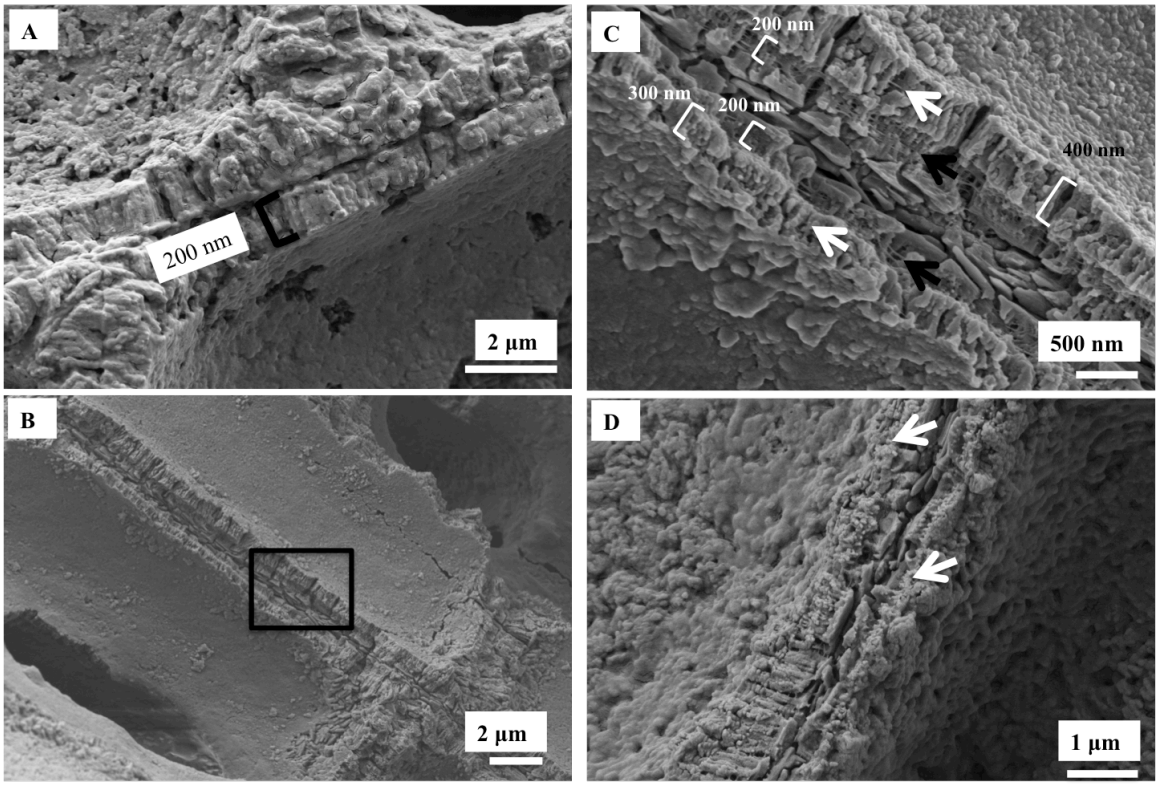

Figure 10: Hypothallus and transitional cells in *L. leave*. Cleaned 2 minutes. **A**. Hypothallus underside. Organic film covering wall structures. Walls ~200 nm wide, roughly radial structure within cell wall. **B**. Cleaned 2 minutes, hypothallus in upper crust. Roughly radial structure within cell walls. Black box enlarged in C. **C**. The wall adjacent to the interfilament is narrowest at ~200 nm, has closely spaced organic fibrils (black arrows) and is poorly calcified compared to the inner part of the wall (300-400 nm wide) where radial grains are present. There are fibrils parallel to the cell wall appearing to go through the wall grains similarly to the perithallial cell walls (white arrows). **D.** Transitional cell wall. The calcification in the lower of the left side wall is comparable to the perithallial cell wall with radial grains. The right side wall and upper part of the left side (white arrows) are poorly calcified and appear as a calcified membrane rather than a properly developed cell wall.